scientific reports

Check for updates

OPEN

Nonlinear excitation of energetic particle driven geodesic acoustic mode by resonance overlap with Alfvén instability in ASDEX Upgrade

Hao Wang[1]✉, Philipp Lauber[2], Yasushi Todo[1]✉, Yasuhiro Suzuki[3], Hanzheng Li[1], Malik Idouakass[1], Jialei Wang[1], Panith Adulsiriswad[4] & The ASDEX Upgrade Team*

The Alfvén instability nonlinearly excited the energetic-particle-driven geodesic acoustic mode on the ASDEX-Upgrade tokamak, as demonstrated experimentally. The mechanism of the energetic-particle-driven geodesic acoustic mode excitation and the mode nonlinear evolution is not yet fully understood. In the present work, a first-principles simulation using the MEGA code investigated the mode properties in both the linear growth and nonlinear saturated phases. Here we show that the simulation successfully reproduced the excitation and coexistence of these two modes, and agreed with the experimental results well. Conclusive evidence showed that the resonance overlap is the excitation mechanism of the energetic-particle-driven geodesic acoustic mode. In the linear growth phase, energetic particles that satisfied different resonance conditions excited the Alfvén instability, which then caused energetic particle redistribution in phase space. These redistributed energetic particles caused resonance overlap, exciting the energetic-particle-driven geodesic acoustic mode in the nonlinear phase.

Alfvén waves are ubiquitous in both laboratory and astrophysical plasmas[1–4]. Alfvén instabilitys are global electromagnetic modes driven by energetic particles, and the spatial profile of Alfvén instability located at the extremum of the shear Alfvén wave continuous spectrum. In the past thirty years, Alfvén instability related theory has been well developed, and Alfvén instabilitys have been observed in many different fusion research experiments[1–5]. Strong energetic particle transport has been observed during Alfvén instability activities, which significantly reduced the effectiveness of plasma heating. The geodesic acoustic mode (GAM) can be seen as the finite frequency electrostatic branch of the zero-frequency zonal $\mathrm{E}\times\mathrm{B}$ flow ($m=0$ and $n=0$) that is generated via side band ($m=\pm1$ and $n=0$) coupling of the poloidal flow to a pressure perturbation, and a parallel ion sound mode.[6–11]. The E is electric field and B is magnetic field. The m and n are the toroidal and poloidal mode numbers. Compared with the GAM, the energetic-particle-driven geodesic acoustic mode (EGAM) takes into account the positive (or negative) contribution of energetic particles to frequency, and it has also been theoretically investigated for many years and has been observed in many devices including tokamaks and stellarators[11–23]. The EGAM also enhances energetic particle transport and can act as an energy channel to anomalously heat bulk plasma[24,25]. It has been found that the EGAM can be excited not only linearly but also nonlinearly. In the Large Helical Device, a low-frequency EGAM can be nonlinearly excited by a high-frequency one[21,22]. Also, it has been found that the GAM can be excited by magnetohydrodynamic (MHD) nonlinearity in a time evolution of the Alfvén eigenmode[26].

Recently, the coexistence of the Alfvén instability and EGAM was found in the ASDEX-Upgrade (AUG) tokamak[27]. In the AUG scenarios of Non-Linear Energetic-particle Dynamics (NLED-AUG) and some similar AUG scenarios, the EGAM appears immediately after the Alfvén instability, and thus the experimentalists believe that the EGAM is triggered by the Alfvén instability. In fact, many simulations have been conducted to

[1]National Institute for Fusion Science, National Institutes of Natural Sciences, Toki 509-5292, Japan. [2]Max-Planck-Institut für Plasmaphysik, 85748 Garching, Germany. [3]Graduate School of Advanced Science and Engineering, Hiroshima University, Higashi-Hiroshima 739-8527, Japan. [4]National Institutes for Quantum Science and Technology, Kamikita 039-3212, Japan. *A list of authors and their affiliations appears at the end of the paper. ✉email: wanghao@nifs.ac.jp; todo@nifs.ac.jp

investigate the NLED-AUG case[28–33]. For example, Poloskei et al. confirms the nonlinear interaction between the Alfvén eigenmode and the EGAMs by using the bicoherence analysis[28]. Vannini et al. demonstrated how energetic particle concentrations affect the Alfvén eigenmode and EGAM under a condition of bump-on-tail distribution, and discussed how the Alfvén eigenmode was excited by the EGAM[29,30]. In addition, based on a slowing-down distribution, they reproduced frequency chirping phenomena very well and the results were very similar to those observed in the experiments[32]. Vlad et al. conducted multi-code simulations to investigate the properties of Alfvén eigenmodes but no code has detected unstable EGAMs in the linear phase, which implies that EGAMs are excited in the nonlinear phase[31]. Rettino et al. conducted ORB5 simulations and found that the EGAM growth rate depends not only on the energetic particle pressure but also sensitively on the energetic particle pitch angle and distribution width[33]. However, the physical mechanism of excitation of the EGAM and the role of energetic particles in nonlinear phase in the shot #34924, an NLED-like case, has not been sufficiently clarified. In the present work, nonlinear simulation is conducted to fill in the above gaps, and the simulation itself includes both the fluid nonlinearity and energetic particle nonlinearity. But only the coupling between Alfvén instability and EGAM via energetic particles is analyzed here, the wave-wave coupling will be analyzed in other works.

In the present work, the EGAM excitation in nonlinear phase by Alfvén instability in AUG is successfully reproduced in the first-principles simulation by using the MEGA code. The fundamental mode properties such as mode frequencies, mode numbers and mode locations are consistent with the experimental results. Also, the radially inward redistribution of energetic particles is qualitatively the same as that in the experiment. The energetic particle distribution is classified into five types of energetic particles distinguished by their magnetic moment μ values and analyzed in (P_ϕ, E) phase space, where P_ϕ is the toroidal canonical momentum and E is energy[34]. In the total distribution f_{total} analysis, the possibility of EGAM excitation is confirmed by checking whether the distribution function is increasing or decreasing with respect to energy on the EGAM resonance region. In the δf distribution analysis, the destabilization and stabilization effects of resonant particles on Alfvén instability and EGAM are carefully investigated. In the linear growth phase, the Alfvén instability resonates with particles. Then, in the nonlinear saturated phase, these resonant particles move in phase space and reach the EGAM resonance region, and cause the overlap of Alfvén instability resonance region and EGAM region. As a result, the EGAM is excited. This excitation mechanism of energetic-particle-driven instabilities through resonance overlap explained the experimental results well.

Results

Both the Alfvén instability and the EGAM are reproduced using the MEGA code, as shown in Fig. 1. Figure 1a shows the poloidal velocity v_θ frequency spectrum simulated using the MEGA code, and Fig. 1b shows the magnetic perturbation frequency spectrum observed in AUG. In Fig. 1a, the Alfvén instability appears at around $t = 0.2$ ms with a frequency of 100 kHz, then it becomes saturated at $t = 0.4$ ms and the frequency starts to chirp up and down. The EGAM appears at around $t = 0.4$ ms with a frequency of 50 kHz, then it becomes saturated at $t \approx 0.65$ ms and the frequency starts to chirp up and down, but the chirping rate lower than the Alfvén instability. The later appearance of the EGAM compared to the Alfvén instability suggests that the EGAM is excited by the Alfvén instability. The mode frequencies of the simulated Alfvén instability and EGAM are similar to the experimental observations shown in Fig. 1b. Moreover, the simulated EGAM saturation level is obviously higher than that of the Alfvén instability, which is also consistent with the observation in Fig. 1b, and this suggests that the excited EGAM is a subcritical instability. In addition, the dominant mode number of the simulated Alfvén instability is $m/n = 3/-1$. Since the Alfvén instability is very close to the Alfvén continuum and almost intersects it, the instability is identified as an energetic-particle-mode (EPM)[35]. The dominant mode numbers of the simulated EGAM are $m/n = 0/0$ for v_θ and 2/0 for magnetic perturbation. The mode numbers are consistent with the theory and experiment[13,18,27,29,33]. Finally, a radially inward energetic particle

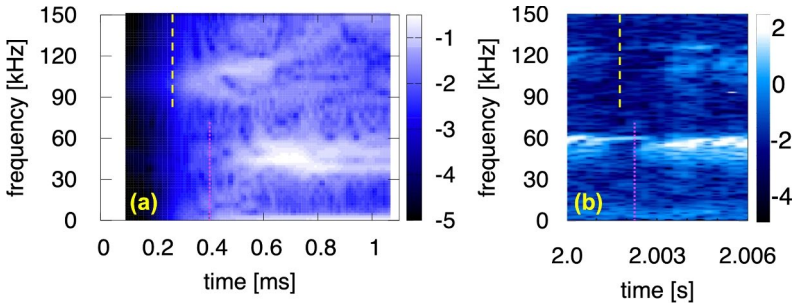

Fig. 1. The reproduction of experimental phenomena by simulation. The frequency spectrum of the Alfvén instability and EGAM are shown, where the Alfvén instability is the higher frequency mode and the EGAM is the lower frequency mode. Panel (**a**) shows the frequency spectrum in the simulation, the color bar represents the velocity perturbation normalized by Alfvén velocity and is plotted on a logarithmic scale. Panel (**b**) shows the experimental observation in shot #34924 of AUG. The color bar represents the soft X-ray emission power and is plotted on a logarithmic scale. Yellow dashed line and pink dotted line represent the excitation time of Alfvén instability and EGAM.

redistribution during mode activities is found in the simulation, which is also consistent with the experiment[27]. The present simulation provides a very good validation.

Both the Alfvén instability and the EGAM can be driven by energetic particles through resonant interactions, if the angular frequency of mode ω_{mode}, the angular frequency of toroidal motion ω_ϕ, and the angular frequency of poloidal motion ω_θ satisfy the resonance condition $\omega_{mode} = n\omega_\phi + L\omega_\theta$ where L is an arbitrary integer. Considering that $n = -1$ for the Alfvén instability and $n = 0$ for the EGAM, the L values are calculated as follows:

$$L_{Alv} = (\omega_{Alv} + \omega_\phi)/\omega_\theta \tag{1}$$

$$L_{EGAM} = \omega_{EGAM}/\omega_\theta \tag{2}$$

The subscript "Alv" represents Alfvén instability. The constant L curves can be plotted in (P_ϕ, E) phase space for specified μ values, where P_ϕ is toroidal canonical momentum. Subsequently, the resonance condition of the resonant particles can be easily analyzed in (P_ϕ, E) space[36,37].

In the present work, slowing-down energetic particle distribution (or negative $\partial f/\partial E$) is applied, and the mode should be stable. However, $\partial f/\partial E$ should be considered with the conserved variables kept constant. One conserved variable is μ which is an adiabatic invariant for the interaction with the Alfvén instability and EGAM whose frequencies are sufficiently lower than the energetic particle gyro-frequency. In addition to μ, $E' = E - \frac{\omega_{AE}}{n} P_\phi$ is a conserved quantity for the Alfvén instability, because $dE/dt = \partial H/\partial t$, $dP_\phi/dt = -\partial H/\partial \phi$, where H is wave field Hamiltonian including the perturbation[4,38,39]. Also, P_ϕ is a conserved quantity for the EGAM because EGAM is an axisymmetric mode with toroidal mode number $n = 0$[13]. Then, positive $\partial f/\partial E$ regions along constant E' and P_ϕ directions should exist. The energetic particle distribution f_{total} is plotted in (P_ϕ, E) phase space to verify the existence of positive $\partial f/\partial E$ regions, as shown in Fig. 2. Three resonance curves where $L_{Alv} = 1$, $L_{Alv} = 0$, and $L_{EGAM} = 1$ are also plotted. Around the EGAM resonance line, the ratio of particle transit frequency to conventional GAM frequency is about 1.25. From the left to the right columns, five cases with different μ values are analyzed as follows. (1) In panels (a1)-(a3), it is clear that $\partial f/\partial E$ is negative along the dotted line and vertical directions on the three resonance curves. Thus, both the Alfvén instability and EGAM may be stabilized. Also, f_{total} does not change too much, this suggests that the resonance of these particles with $\mu = 1.62 keV/T$ may be not strong. (2) In panels (b1)-(b3), the EGAM may be stabilized with

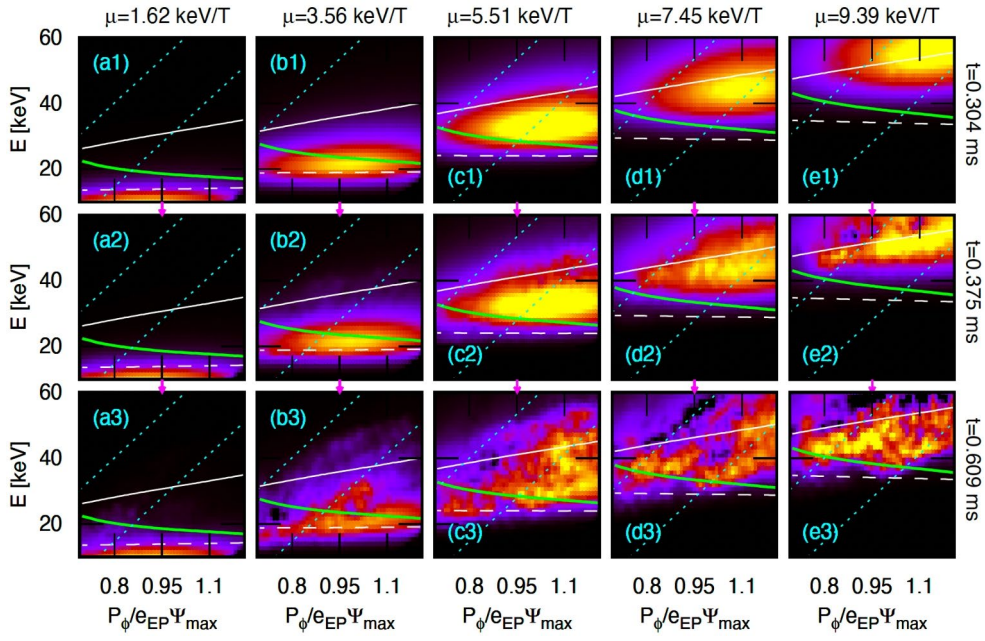

Fig. 2. The resonance overlap illustrated by the energetic particle distribution f_{total} in phase space. The f_{total} in (P_ϕ, E) phase space for different μ values at different times are shown. P_ϕ is normalized to the product of particle charge e_{EP} and the maximum ψ at the plasma center. From the top to the bottom, the three rows are plotted at $t = 0.304$ ms, 0.375 ms, and 0.609 ms, respectively. From the left to the right, the five columns represent different μ values of 1.62, 3.56, 5.51, 7.45 and 9.39 with unit keV/T, respectively. The black color represents the minimum f_{total} value 0. The bright yellow color represents the maximum f_{total} values, and in the five columns from the left to the right, they are 30, 12, 5, 4, and 2.5, respectively. The solid and dashed white curves represent respectively $L_{Alv} = 1$ and 0, and the green curve represents $L_{EGAM} = 1$. The two cyan dotted lines represent two constant E' values. The constant P_ϕ lines are not plotted because they are parallel to the vertical axis.

$L_{EGAM} = 1$, but the Alfvén instability may be simultaneously stabilized with $L_{Alv} = 1$ and destabilized with $L_{Alv} = 0$. (3) In panels (c1)-(c3), the EGAM may be destabilized with $L_{EGAM} = 1$, but the Alfvén instability may be simultaneously stabilized with $L_{Alv} = 1$ and destabilized with $L_{Alv} = 0$. (4) In panels (d1)-(d3), the EGAM may be destabilized with $L_{EGAM} = 1$, and the Alfvén instability may be destabilized with $L_{Alv} = 0$. For $L_{Alv} = 1$, it is difficult to draw a conclusion because the sign of $\partial f/\partial E$ may be different in low P_ϕ and high P_ϕ regions. (5) In panels (e1)-(e3), both the Alfvén instability and EGAM may be destabilized. In addition, f_{total} changes drastically in many panels, especially in the second and third rows, this indicates very strong particle-wave interactions. Also, f_{total} is redistributed along the direction of the dotted lines, which indicates that the particles are resonant with the Alfvén instability. A more detailed evolution of the above five cases can be found in supplementary movie 1-5.

The time evolution of the energetic particle distribution f_{total} along the constant E' line and the constant P_ϕ line are shown in Fig. 3 to better illustrate the redistribution, where the particle μ value is 7.45 keV/T . Fig. 3a and c show f_{total} along the right (or lower) E' line of Fig. 2. The significant differences of the f_{total} at $\mathrm{t} = 0.3\mathrm{ms}$ and $\mathrm{t} = 0.8\mathrm{ms}$ indicate a strong redistribution, and the increase of f_{total} on the $L_{EGAM} = 1$ resonance layer (cyan line in Fig. 3a) implies the interactions between energetic particles and EGAM. Fig. 3b and d show f_{total} along the vertical line of Fig. 2, with a $P_\phi/e_{EP}\psi_{max}$ value of 0.778. Similar to Fig. 3a and c, the significant differences of the f_{total} at different times indicate a strong redistribution, and the drastic changes of f_{total} in the $L_{EGAM} = 1$ resonance layer (cyan line in Fig. 3b) imply the excitation of EGAM. In order to better

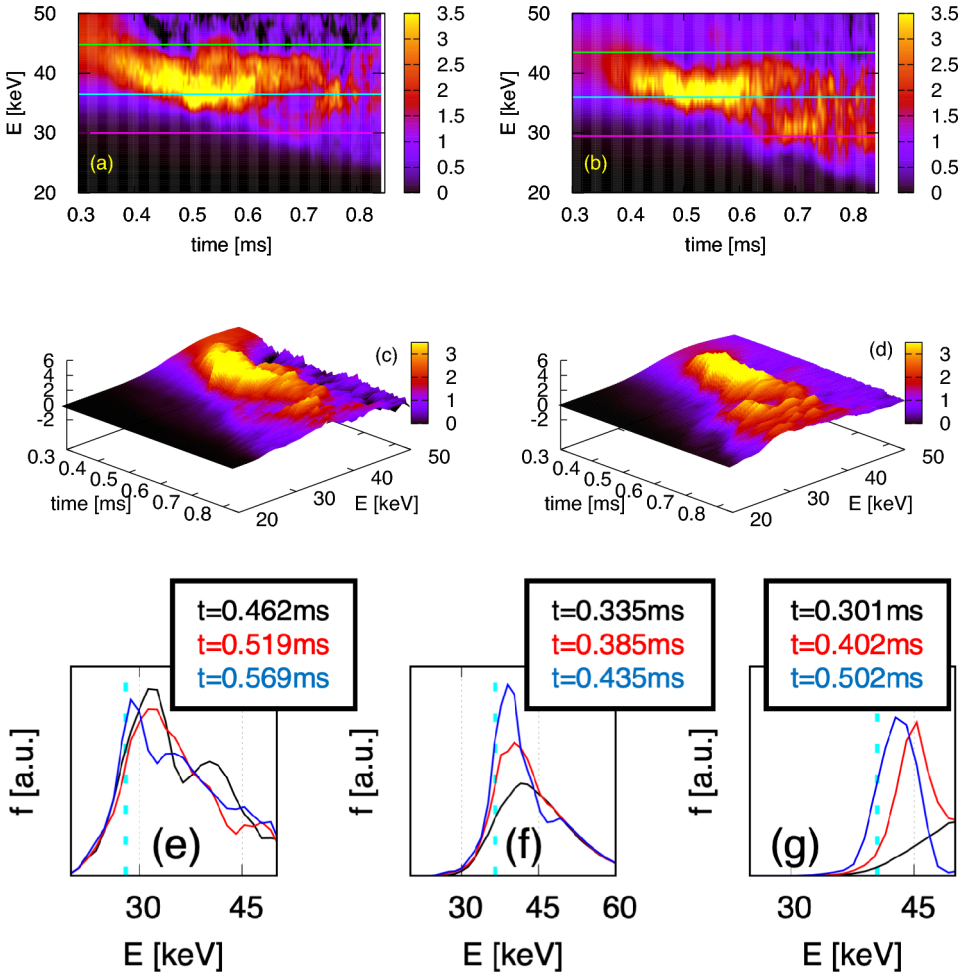

Fig. 3. The resonance overlap illustrated by the energetic particle distribution f_{total} with detailed time evolution. The time evolution of f_{total} along (**a**) the left (or higher) E' line of Fig. 2 and (**b**) the vertical line of Fig. 2 with a $P_\phi/e_{EP}\psi_{max}$ value of 0.778, are shown in details. The particle μ value is 7.45 keV/T . These three horizontal lines from top to bottom represent three resonant layers of $L_{Alv} = 1$, $L_{EGAM} = 1$, and $L_{Alv} = 0$, respectively. To better understand the physical pictures described above, the bird's-eye view 3-dimensional sub-figures are also presented. The sub-figures (**c**) and (**d**) correspond to the sub-figures (**a**) and (**b**), respectively, and their vertical axes represent f_{total}. The sub-figures (**e**–**g**) show the f_{total} along $P_\phi = const.$ at different times, the $P_\phi/e_{EP}\psi_{max}$ values are 0.994, 0.778, and 0.804, the maximum values of the vertical axis are 6.5, 3.5 and 3.5, and the particle μ values are 5.51, 7.45 and 9.39 keV/T, respectively. The vertical dotted lines represent the resonant layers of $L_{EGAM} = 1$.

demonstrate the change of $\partial f/\partial E$, the f_{total} along $P_\phi = const.$ at different times are plotted in Fig. 3e–g. The changes of $\partial f/\partial E$ implies the destabilization of EGAM.

The possibility of EGAM excitation can be confirmed from Figs. 2 and 3, but the detailed mechanism of EGAM excitation is not demonstrated. In order to gain further insights, $\delta f = f_{total} - f_{total\ at\ t=0}$ distribution[40] is plotted in (P_ϕ, E) phase space in Fig. 4, where $\frac{d}{dt}\delta f = -\frac{dE}{dt}\frac{\partial f_{total\ at\ t=0}}{\partial E} - \frac{dP_\phi}{dt}\frac{\partial f_{total\ at\ t=0}}{\partial P_\phi}$[19] and non-zero δf represents particle redistribution. A mode is destabilized if a negative δf region appears above the resonance curve and a positive one appears below the resonance curve. On the contrary, a mode is stabilized if a negative δf region appears below the resonance curve and a positive one appears above. Then, a pair of positive and negative δf regions form a resonance region. From the left to the right columns in Fig. 4, five cases with different μ values are analyzed as follows. (1) In panels (a1)-(a3), the Alfvén instability is stabilized with $L_{Alv} = 0$. (2) In panels (b1)-(b3), the Alfvén instability is destabilized with $L_{Alv} = 0$, then, the EGAM is stabilized with $L_{EGAM} = 1$. (3) In panels (c1)-(c3), the Alfvén instability is stabilized with $L_{Alv} = 1$. Then, during the Alfvén instability frequency chirping, the resonance regions move from the black Alfvén instability resonance curve (c1) to the position slightly below the black curve (c2) along the dotted line, and finally, move to the red EGAM resonance curve (c3), and as a result, the EGAM is destabilized with $L_{EGAM} = 1$. The EGAM excitation by the resonance overlap with Alfvén instability is demonstrated in this process. (4) In panels (d1)-(d3), the Alfvén instability is destabilized with $L_{Alv} = 1$. Then, during the Alfvén instability frequency chirping, the resonance regions move from the black Alfvén instability resonance curve (d1) to the position slightly below the black curve (d2), and finally, move to the red EGAM resonance curve (d3) and the EGAM is destabilized with $L_{EGAM} = 1$. Similar to the case of the third column, the EGAM excitation by the resonance overlap with Alfvén instability is demonstrated in this process. (5) In panels (e1)-(e3), the Alfvén instability is destabilized with $L_{Alv} = 1$. In the resonance overlap process described above, the area of the resonance region continues to expand. This expansion occurs not only in the direction from the L_{Alv} layer towards the L_{EGAM} layer, but also in the opposite direction, moving away from the L_{Alv} layer towards the L_{EGAM} layer. When the resonance region is located between the L_{Alv} and L_{EGAM} resonance layers, the energy of the particles is only used to overcome the damping and maintain the amplitude of the Alfvén instability. In addition, the differences of δf at $t = 0.539$ ms and 0.727 ms for particles with μ values of 1.62 and 9.39 keV/T are examined. It is found that EGAM is slightly stabilized with $L_{EGAM} = 1$ and slightly destabilized with $L_{EGAM} = 2$ by particles with $\mu = 1.62\text{keV/T}$, although $L_{EGAM} = 2$ is not shown in Fig. 4. Also, EGAM is slightly destabilized with $L_{EGAM} = 1$ by particles with $\mu = 9.39\text{keV/T}$. A more detailed evolution of the above five cases can be found in supplementary movie 6-10.

Based on the above results, the destabilization and stabilization effects of resonant particles on the Alfvén instability and EGAM are clearly demonstrated. The findings are summarized in Table 1.

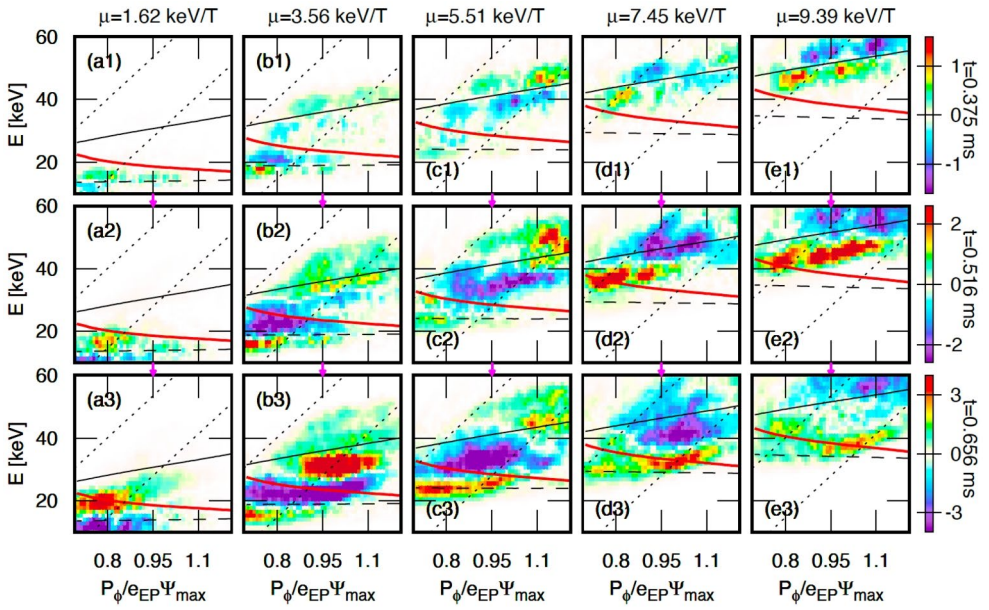

Fig. 4. The resonance overlap illustrated by the energetic particle distribution δf in phase space. The δf in (P_ϕ, E) phase space for different μ values at different times are shown. P_ϕ is normalized to the product of particle charge e_{EP} and the maximum ψ at the plasma center. From the top to the bottom, the three rows are plotted at $t = 0.375$ ms, 0.516 ms and 0.656 ms, respectively. From the left to the right, the five columns represent different μ values of 1.62, 3.56, 5.51, 7.45 and 9.39 with unit keV/T, respectively. The red color represents positive δf and the blue represents negative δf. The solid and dashed black curves represent respectively $L_{Alv} = 1$ and 0, and the red curve represents $L_{EGAM} = 1$. The two black dotted lines represent two constant E' values. The constant P_ϕ lines are not plotted because they are parallel to the vertical axis.

μ [keV/T]	Alfvén instability	L_{Alv}	EGAM	L_{EGAM}
1.620	Stabilized	0	Weak	1, 2
3.561	Destabil. & Stabil.	0 & 1	Stabilized	1
5.509	Stabilized	1	Destabilized	1
7.450	Destabilized	1	Destabilized	1
9.392	Destabilized	1	Weak	1

Table 1. The effects of particles on Alfvén instability and EGAM.

Discussion

The results above demonstrate that the MEGA simulation successfully reproduced the excitation of EGAM in nonlinear phase by Alfvén instability in AUG. The simulation matches the experimental results well. By analyzing the evolution of energetic particles in the (P_ϕ, E) phase space, the resonance overlap is identified as the excitation mechanism of EGAM. In the f_{total} figure, EGAM can be excited since $\partial f/\partial E > 0$ in the EGAM resonance region. In the δf figure, the pair of positive and negative δf values in the Alfvén instability and EGAM resonance region indicates the destabilization and stabilization of the modes. Particles are divided into 5 categories based on their respective μ values, and those particles with μ values around 7.5 keV/T are particularly significant as they play an important role in the excitation of the EGAM in nonlinear phase. Initially, these particles located in the Alfvén instability resonance region excite Alfvén instability in the linear growth phase, and then, during the nonlinear saturated phase, these resonant particles move in phase space and reach the EGAM resonance region. As a result, the EGAM is excited by resonance overlap.

The resonance overlap process can be summarized as follows[5]. Initially, particles resonate with the first instability, and as the mode amplitude grows, the size of the resonance region expands in phase space. Eventually, the first instability resonance region becomes very large, and reaches the second instability resonance region. The first instability resonance region overlaps with the second instability resonance region, and the second instability is excited. After the fractional resonance[22] was clarified, the resonance overlap[5] is another physical mechanism to nonlinearly excite EGAM through energetic particle.

It is worth noting that the EGAM cannot be excited in burning plasma without auxiliary heating due to the isotropic α-particle distribution, but in the present work, it is demonstrated that even in burning plasma without auxiliary heating the EGAM may still be excited by the Alfvén instability if the finite width or the shift of the Alfvén instability resonance region results in the resonance overlap with the EGAM. The width of the resonance region increases for larger amplitude of the Alfvén instability while the frequency chirping is associated with the shift of the resonance region in phase space. Due to the difference in the toroidal mode numbers of the Alfvén instability and EGAM, even if the frequencies of the Alfvén instability and EGAM differ greatly, the resonance curves of these two modes may still be close to each other in the phase space. Then, even for a small change in Alfvén instability frequency in the nonlinear stage, the energetic particle phase space redistribution may induce a strong EGAM excitation. Since EGAM can anomalously heat bulk plasma by creating an energy channel[11,24,25], for burning plasma, EGAM may not only play a negative role (enhanced transport) but also play a positive role (anomalous heating).

The nonlinear interactions between Alfvén instabilitys and between Alfvén instabilitys and EGAM are ubiquitous in fusion plasmas[3,26,41,42] and important for plasma confinement due to the enhanced energetic particle transport and EGAM channeling. In this work, the mechanism of EGAM being excited by Alfvén instability on AUG is clarified, and more importantly, the method adopted in this work to analyze particle resonance conditions in phase space can be used for a wide range of mode-particle-mode interactions. The excitation mechanism through resonance overlap, as described in this work, could potentially explain other phenomena involving mode-particle-mode interactions, even those outside of fusion plasmas. For example, in the space plasmas, it has been observed that the cross-energy couplings from magnetosonic waves to electromagnetic ion cyclotron waves through cold ion heating[43]. It is demonstrated that the magnetosonic waves excited by high-energy ($>$ 1 keV) ions heat cold ions leading to the excitation of electromagnetic ion cyclotron waves. The process demonstrated in the present paper (particle $\rightarrow$ Alfvén wave $\rightarrow$ particle $\rightarrow$ EGAM wave) is similar to that in Ref.[43] (particle $\rightarrow$ magnetosonic wave $\rightarrow$ particle $\rightarrow$ cyclotron wave), although the energy of EGAM does not derive entirely from Alfvén instability due to the inherent feature of subcritical instability. Consequently, the approach outlined in the present paper might also be applicable to space plasma.

Finally, as mentioned in the introduction section, the wave-wave nonlinearity also contributes to the mode excitation[28,30] in the NLED case. In the present work of shot #34924, in addition to the energetic particle nonlinearity, the wave-wave nonlinearity should also be investigated given its high importance.

Methods

ASDEX-upgrade

The ASDEX-Upgrade is a magnetic confinement fusion facility based on the tokamak concept operated by the Max-Planck-Institute for plasma physics in Garching, Germany. The full name of ASDEX is "Axially Symmetric Divertor EXperiment". The magnetic system of ASDEX-Upgrade consists of 16 toroidal field coils and 12 poloidal field coils. The toroidal magnetic field strength is up to 3.1 T, and the major radius is 1.65 m. The plasma volume is 13 m^3.

MEGA code

MEGA[26,44], a first-principles hybrid simulation code for energetic particles interacting with an MHD fluid, is used to simulate the coexistence of the Alfvén instability and EGAM. In the MEGA code, bulk plasma is described by nonlinear MHD equations. The drift kinetic description and the δf particle-in-cell method are applied to the energetic particles. The 4th-order Runge-Kutta algorithm and 4th-order finite differential algorithm are applied in the code. The energetic particles and the MHD are coupled via the current in the momentum equation. After the initial parameters are loaded, plasma properties and behavior in the MEGA code evolve based on MHD equations and kinetic equations, without relying on empirical data.

Equilibrium data

A realistic equilibrium constructed using the EFIT code[45] is used for the simulation. EFIT, which stands for Equilibrium FITting, is a widely-used code for reconstructing the equilibrium state of a tokamak plasma. It was developed several decades ago and has since become a standard tool in the field of fusion research. This equilibrium data is based on AUG shot #34924 at time $t = 1.90$ s. From $t = 1.90$ s to $t = 2.01$ s, plasma parameters and profiles remain constant within the error bars.

Energetic particle distribution function

In the NLED-AUG case, according to NUBEAM data, the energetic particle distribution function is a roughly slowing-down type in phase space and a Gaussian type in pitch angle space. Then, in the present work, similar types of distribution are assumed. Here, the NUBEAM code[46] is a simulation tool used for Neutral Beam Injection (NBI) in tokamaks. It computes the time-dependent deposition and slowing-down of the fast ions produced by NBI. The energetic particle velocity distribution is $f(v) = \frac{1}{v^3+v_c^3}$, where v is the velocity and v_c is the critical velocity. The collisions with electrons dominate the slowing-down process if the particle velocity is above v_c, while for $v < v_c$, the slowing-down is mainly due to collisions with background ions. The energetic particle pitch angle distribution is $g(\Lambda) = \exp[-(\Lambda - \Lambda_{peak})^2/\Delta\Lambda^2]$, where Λ is defined by $\mu B_0/E$, μ is the magnetic moment, B_0 is the magnetic strength on the axis, E is the energy, $\Lambda_{peak} = 0.4$ represents the pitch angle for the distribution peak, and $\Delta\Lambda = 0.1$ is a parameter to control the distribution width. In addition, the energetic particle radial profile peaks around $r/a = 0.5$ in shot #34924, and accordingly, the radial distribution in the simulation is $h(\psi) = \exp[-(\psi_{nrm} - \psi_{peak})^2/\Delta\psi^2]$, where ψ is the poloidal magnetic flux, ψ_{nrm} is ψ normalized by the maximum value, $\psi_{peak} = 0.73$ is a parameter to control the radial peak location, and $\Delta\psi = 0.274$ is another parameter to control the radial width.

Simulation parameters

The parameters for the simulation are also based on AUG shot #34924. These are $B_0 = 2.49$ T, electron density $n_e = 1.78 \times 10^{19}$ m^{-3} at the axis, and electron temperature $T_e = 1.5$ keV at the axis. The injected neutral beam energy is $E_{NBI} = 93$ keV. Both the bulk plasma and energetic particles are deuterium. The safety factor q profile has weak shear in the core region, with the value 2.3 at the magnetic axis and 6.43 at the plasma edge. The major radius of the magnetic axis is $R_0 = 1.686$ m. Cylindrical coordinates (R, ϕ, z) are employed. The numbers of grid points in (R, ϕ, z) directions are (128, 32, 256), respectively.

Data availability

The data supporting the results of this study are available upon request from the first and second authors (H.W. for simulations and Ph.L. for experiments). The data are not publicly available due to regulations of National Institute for Fusion Science (NIFS) and Max Planck Institute for Plasma Physics (IPP). Before the data can be released, an official research collaboration agreement with NIFS and IPP must be established.

Code availability

Further information and the source code of MEGA[44] is available from the corresponding authors upon reasonable request.

Received: 8 May 2024; Accepted: 6 December 2024
Published online: 07 January 2025

References

1. Heidbrink, W. & Sadler, G. The behaviour of fast ions in tokamak experiments. *Nucl. Fusion* **34**, 535 (1994).
2. Heidbrink, W. Basic physics of alfven instabilities driven by energetic particles in toroidally confined plasmas. *Phys. Plasmas* **15**, 055501 (2008).
3. Chen, L. & Zonca, F. Physics of alfvén waves and energetic particles in burning plasma. *Rev. Modern Phys.* **88**, 015008 (2016).
4. Todo, Y. Introduction to the interaction between energetic particles and alfven eigenmodes in toroidal plasmas. *Rev. Mod. Plasma Phys.* **3**, 1 (2019).
5. Todo, Y.: Critical energetic particle distribution in phase space for the alfvÃ©n eigenmode burst with global resonance overlap. Nucl. Fusion, 096048 (2019)
6. Winsor, N., Johnson, J. L. & Dawson, J. M. Geodesic acoustic waves in hydromagnetic systems. *Phys. Fluids* **11**, 2448–2450 (1968).
7. Diamond, P. H., Itoh, S.-I., Itoh, K. & Hahm, T. S. Zonal flows in plasma–a review. *Plasma Phys. Controlled Fusion* **47**(5), 35 (2005).
8. Sugama, H. & Watanabe, T.-H. Collisionless damping of zonal flows in helical systems. *Phys. Plasmas* **13**(1), 012501–01250118 (2006).
9. Zonca, F. & Chen, L. Radial structures and nonlinear excitation of geodesic acoustic modes. *Europhys. Lett.* **83**, 35001 (2008).
10. Souza, F. C., Gorelenkov, N., Elfimov, A. & GalvÃ£o, R., Collins, C., Podesta, M., Fredrickson, E.,. Description of global egam in the maximum of local frequency during current ramp-up discharges in diii-d. *J. Plasma Phys.* **88**(3), 905880308 (2022).

11. Conway, G. D., Smolyakov, A. I. & Ido, T. Geodesic acoustic modes in magnetic confinement devices. *Nucl. Fusion* **62**, 013001 (2022).
12. Berk, H. L. et al. JET EFDA contributors: Explanation of the jet n = 0 chirping mode. *Nucl. Fusion* **46**(10), 888 (2006).
13. Fu, G. Y. Energetic-particle-induced geodesic acoustic mode. *Phys. Rev. Lett.* **101**, 185002 (2008).
14. Nazikian, R. et al. Intense geodesic acousticlike modes driven by suprathermal ions in a tokamak plasma. *Phys. Rev. Lett.* **101**, 185001 (2008).
15. Qiu, Z., Zonca, F. & Chen, L. Nonlocal theory of energetic-particle-induced geodesic acoustic mode. *Plasma Phys. Controlled Fusion* **52**(9), 095003 (2010).
16. Kramer, G. J. et al. Fractional resonances between waves and energetic particles in tokamak plasmas. *Phys. Rev. Lett.* **109**, 035003 (2012).
17. Zarzoso, D., Garbet, X., Sarazin, Y., Dumont, R. & Grandgirard, V. Fully kinetic description of the linear excitation and nonlinear saturation of fast-ion driven geodesic acoustic mode instability. *Phys. Plasmas* **19**, 022102 (2012).
18. Wang, H. & Todo, Y. Linear properties of energetic particle driven geodesic acoustic mode. *Phys. Plasmas* **20**(1), 012506 (2013).
19. Wang, H., Todo, Y. & Kim, C. C. Hole-clump pair creation in the evolution of energetic-particle-driven geodesic acoustic modes. *Phys. Rev. Lett.* **110**(15), 155006 (2013).
20. Girardo, J. et al. Relation between energetic and standard geodesic acoustic modes. *Phys. Plasmas* **21**, 092507 (2014).
21. Ido, T. et al. LHD Experiment Group: Strong destabilization of stable modes with a half-frequency associated with chirping geodesic acoustic modes in the large helical device. *Phys. Rev. Lett.* **116**(1), 015002 (2016).
22. Wang, H., Todo, Y., Ido, T. & Suzuki, Y. Chirping and sudden excitation of energetic-particle-driven geodesic acoustic modes in a large helical device experiment. *Phys. Rev. Lett.* **120**, 175001 (2018).
23. Falessi, M., Chen, L., Qiu, Z. & Zonca, F. Nonlinear equilibria and transport processes in burning plasmas. *New J. Phys.* **25**, 123035 (2023).
24. Osakabe, M., Ido, T., Ogawa, K., Shimizu, A., Yokoyama, M., Seki, R., Suzuki, C., Isobe, M., Toi, K., Spong, D.A., Nagaoka, K., Takeiri, Y., Igami, H., Seki, T., Nagasaki, K., LHD Experiment Group: Indication of Bulk-ion Heating by Energetic Particle Driven Geodesic Acoustic Modes on LHD. In: 25th IAEA Fusion Energy Conference Proceedings (2014).
25. Wang, H., Todo, Y., Oasakabe, M., Ido, T. & Suzuki, Y. Simulation of energetic particle driven geodesic acoustic modes and the energy channeling in the large helical device plasmas. *Nucl. Fusion* **59**, 096041 (2019).
26. Todo, Y., Berk, H. L. & Breizman, B. N. Nonlinear magnetohydrodynamic effects on alfven eigenmode evolution and zonal flow generation. *Nucl. Fusion* **50**(8), 084016 (2010).
27. LAUBER, P., GEIGER, B., PAPP, G., POR, G., L.GUIMARAIS, POLOSKEI, P., IGOCHINE, V., MARASCHEK, M., POKOL, G., HAYWARD-SCHNEIDER, T., LU, Z., WANG, X., BOTTINO, A., PALERMO, F., NOVIKAU, I., BIANCALANI, A., G.CONWAY, THE ASDEX UPGRADE TEAM, THE EUROFUSION ENABLING RESEARCH 'NAT' AND 'NLED' TEAMS: STRONGLY NON-LINEAR ENERGETIC PARTICLE DYNAMICS IN ASDEX UPGRADE SCENARIOS WITH CORE IMPURITY ACCUMULATION. In: 27th IAEA Fusion Energy Conference Proceedings (2018).
28. Poloskei, P., Papp, G., Pokol, G., Lauber, P., Wang, X., Horvath, L., THE ASDEX UPGRADE TEAM: Bicoherence Analysis of Fast Ion Driven Transient Plasma Waves. In: 44th EPS Conference on Plasma Physics (2017).
29. Vannini, F. et al. ASDEX Upgrade Team: Gyrokinetic investigation of the damping channels of alfven modes in ASDEX Upgrade. *Phys. Plasmas* **27**, 042501 (2020).
30. Vannini, F. et al. ASDEX Upgrade Team: Gyrokinetic investigation of the nonlinear interaction of alfven instabilities and energetic particle-driven geodesic acoustic modes. *Phys. Plasmas* **28**, 072504 (2021).
31. Vlad, G. et al. A linear benchmark between hymagyc, mega and orb5 codes using the NLED-AUG test case to study alfvénic modes driven by energetic particles. *Nucl. Fusion* **61**, 116026 (2021).
32. Vannini, F. et al. ASDEX Upgrade Team: Gyrokinetic modelling of the alfven mode activity in ASDEX Upgrade with an isotropic slowing-down fast-particle distribution. *Nucl. Fusion* **62**, 126042 (2022).
33. Rettino, B. et al. Gyrokinetic modeling of anisotropic energetic particle driven instabilities in tokamak plasmas. *Nucl. Fusion* **62**, 076027 (2022).
34. White, R. B. *Theory of Tokamak Plasmas* 2nd edn. (Imperial College Press, London, 2001).
35. Wang, H. et al. Nonlinear excitation of energetic particle driven geodesic acoustic mode by alfvén instability in asdex-upgrade tokamak. *Nucl. Fusion* **64**, 076015 (2024).
36. Todo, Y., Sato, M., Wang, H., Idouakass, M. & Seki, R. Magnetohydrodynamic hybrid simulation model with kinetic thermal ions and energetic particles. *Plasma Phys. Control. Fusion* **63**, 075018 (2021).
37. Li, H., Todo, Y., Wang, H., Idouakass, M. & Wang, J. Simulation study of energetic-particle driven off-axis fishbone instabilities in tokamak plasmas. *Nucl. Fusion* **62**(2), 026013 (2022).
38. Hus, C. T. & Sigmar, D. J. Alpha-particle losses from toroidicity-induced alfven eigenmodes. Part i: Phase-space topology of energetic particle orbits in tokamak plasma. *Phys. Fluids B* **4**(6), 1492 (1992).
39. Heidbrink, W. & White, R. B. Mechanisms of energetic-particle transport in magnetically confined plasmas. *Phys. Plasmas* **27**, 030901 (2020).
40. Aydemir, A. Y. A unified monte carlo interpretation of particle simulations and applications to non-neutral plasmas. *Phys. Plasmas* **1**(4), 822 (1993).
41. Lauber, P. Local and global kinetic stability analysis of alfvén eigenmodes in the 15 MA ITER scenario. *Plasma Phys. Control. Fusion* **57**, 054011 (2015).
42. Qiu, Z., Chen, L., Zonca, F. & Chen, W. Nonlinear excitation of a geodesic acoustic mode by toroidal alfvÃn eigenmodes and the impact on plasma performance. *Nucl. Fusion* **59**(6), 066031 (2019).
43. Asamura, K. et al. Cross-energy couplings from magnetosonic waves to electromagnetic ion cyclotron waves through cold ion heating inside the plasmasphere. *Phys. Rev. Lett.* **127**(24), 245101 (2021).
44. Todo, Y. et al. Comprehensive magnetohydrodynamic hybrid simulations of fast ion driven instabilities in a large helical device experiment. *Phys. Plasmas* **24**(8), 081203 (2017).
45. Lao, L., John, H., Stambaugh, R., Kellman, A. & Pfeiffer, W. Reconstruction of current profile parameters and plasma shapes in tokamaks. *Nucl. Fusion* **25**, 1611 (1985).
46. Pankin, A., McCune, D., Andre, R., Bateman, G. & Kritz, A. The tokamak monte carlo fast ion module nubeam in the national transport code collaboration library. *Comput. Phys. Commun.* **159**, 157 (2004).

Acknowledgements

Numerical computations were performed on the "Plasma Simulator" (NEC SX-Aurora TSUBASA) of National Institute for Fusion Science (NIFS) with the support and under the auspices of the NIFS Collaboration Research program (NIFS19KNXN397, NIFS20KNST156, NIFS21KNST196, and NIFS22KIST025), the JFRS-1 supercomputer system at Computational Simulation Centre of International Fusion Energy Research Centre (IFERC-CSC), and the Supercomputer Fugaku provided by the RIKEN Center for Computational Science (Project IDs: hp200127, hp210178, hp220165). This work was partially supported by MEXT as "Program for Promoting Researches on the Supercomputer Fugaku (Exploration of burning plasma confinement physics, JP-

MXP1020200103)", JSPS KAKENHI Grant Nos. JP18K13529, JP18H01202, JP21H04973, and "PLADyS", JSPS Core-to-Core Program, A. Advanced Research Networks. Also, This work was partially supported by the NINS program of Promoting Research by Networking among Institutions (Grant Number 01422301) and by the International Research Exchange Support Program of the National Institutes of Natural Sciences. In addition, this work was partially carried out within the framework of the EUROfusion Consortium, funded by the European Union via the Euratom Research and Training Programme (Grant Agreement No. 101052200 - EUROfusion). Views and opinions expressed are however those of the author(s) only and do not necessarily reflect those of the European Union or the European Commission. Neither the European Union nor the European Commission can be held responsible for them. The authors thank Prof. K. Nagasaki of Kyoto Univ., Dr. T. Hayward-Schneider of MPG-IPP, Mr. B. Rettino of MPG-IPP, Dr. F. Vannini of MPG-IPP, Dr. Z. Lu of MPG-IPP, Dr. X. Wang of MPG-IPP, Dr. G. Meng of MPG-IPP, Prof. S. Okamura of NIFS, Prof. M. Osakabe of NIFS, Prof. K. Ida of NIFS, Prof. K. Ichiguchi of NIFS for their sincere help and fruitful discussions.

Author contributions

H.W. performed the simulations and data analysis, and wrote the manuscript with help from Y.T. for simulation and Ph.L. for experiment. Ph.L. provided the experimental data. Y.T. developed the code MEGA and motivated crucial steps that have moved this research forward. Y.S. funded H.W.'s visit to IPP. H.L. helped with the data analysis in phase space. All authors, including those mentioned above, participated in the discussion and interpretation of the results from simulations and experiments.

Declarations

Competing interests

The authors declare no competing interests.

Additional information

Supplementary Information The online version contains supplementary material available at https://doi.org/10.1038/s41598-024-82577-3.

Correspondence and requests for materials should be addressed to H.W. or Y.T.

Reprints and permissions information is available at www.nature.com/reprints.

Publisher's note Springer Nature remains neutral with regard to jurisdictional claims in published maps and institutional affiliations.

The ASDEX Upgrade Team

H. Zohm[2], E. Alessi[15], C. Angioni[2], N. Arden[2], V. Artigues[2], M. Astrain[2], O. Asunta[7], M. Balden[2], V. Bandaru[2], A. Banon Navarro[2], M. Bauer[2], A. Bergmann[2], M. Bergmann[2], J. Bernardo[6], M. Bernert[2], A. Biancalani[45], R. Bielajew[44], R. Bilato[2], G. Birkenmeier[2,10], T. Blanken[8], V. Bobkov[2], A. Bock[2], L. Bock[2], T. Body[2], T. Bolzonella[11], N. Bonanomi[2], A. Bortolon[35], B. Böswirth[2], C. Bottereau[12], A. Bottino[2], H. van den Brand[8], M. Brenzke[13], S. Brezinsek[13], D. Brida[2], F. Brochard[14], J. Buchanan[9], A. Buhler[2], A. Burckhart[2], Y. Camenen[54], B. Cannas[41], P. Cano Megías[2], D. Carlton[2], M. Carr[9], P. Carvalho[6], C. Castaldo[53], A. Castillo Castillo[2], A. Cathey[2], M. Cavedon[47], C. Cazzaniga[11], C. Challis[9], A. Chankin[2], A. Chomiczewska[19], C. Cianfarani[53], F. Clairet[12], S. Coda[16], R. Coelho[6], J. W. Coenen[13], L. Colas[12], G. Conway[2], S. Costea[17], D. Coster[2], T. Cote[49], A. J. Creely[44], G. Croci[15], D. J. Cruz Zabala[23], G. Cseh[18], I. Cziegler[33], O. D'Arcangelo[37], A. Dal Molin[47], P. David[2], C. Day[20], M. de Baar[8], P. de Marné[2], R. Delogu[11], P. Denner[13], A. Di Siena[2], M. Dibon[2], J. J. Dominguez-Palacios Durán[23], D. Dunai[18], M. Dreval[55], M. Dunne[2], B. P. Duval[16], R. Dux[2], T. Eich[2], S. Elgeti[2], A. Encheva[46], B. Esposito[53], E. Fable[2], M. Faitsch[2], D. Fajardo Jimenez[2], U. Fantz[2], M.

Farnik[48], H. Faugel[2], F. Felici[16], O. Ficker[48], A. Figueredo[6], R. Fischer[2], O. Ford[5], L. Frassinetti[21], M. Fröschle[2], G. Fuchert[5], J. C. Fuchs[2], H. Fünfgelder[2], S. Futatani[36], K. Galazka[19], J. Galdon-Quiroga[23], D. Gallart Escolà[36], A. Gallo[12], Y. Gao[13], S. Garavaglia[15], M. Garcia Munöz[23], B. Geiger[49], L. Giannone[2], S. Gibson[52], L. Gil[6], E. Giovannozzi[53], I. Girka[2], O. Girka[2], T. Gleiter[2], S. Glöggler[2,10], M. Gobbin[11], J. C. Gonzalez[2], J. Gonzalez Martin[23], T. Goodman[16], G. Gorini[47], T. Görler[2], D. Gradic[5], G. Granucci[15], A. Gräter[2], G. Grenfell[2], H. Greuner[2], M. Griener[2], M. Groth[7], O. Grover[2], A. Gude[2], L. Guimarais[6], S. Günter[2], D. Hachmeister[6], A. H. Hakola[24], C. Ham[9], T. Happel[2], N. den Harder[2], G. Harrer[32], J. Harrison[9], V. Hauer[20], T. Hayward-Schneider[2], B. Heinemann[2], P. Heinrich[2], T. Hellsten[22], S. Henderson[9], P. Hennequin[26], M. Herschel[2], S. Heuraux[14], A. Herrmann[2], E. Heyn[56], F. Hitzler[2,10], J. Hobirk[2], K. Höfler[5], S. Hörmann[2], J. H. Holm[28], M. Hölzl[2], C. Hopf[2], L. Horvath[33], T. Höschen[2], A. Houben[14], A. Hubbard[44], A. Huber[13], K. Hunger[2], V. Igochine[2], M. Iliasova[43], J. Illerhaus[2], K. Insulander Björk[50], C. Ionita-Schrittwieser[17], I. Ivanova-Stanik[19], S. Jachmich[46], W. Jacob[2], N. Jaksic[2], A. Jansen van Vuuren[23], F. Jaulmes[48], F. Jenko[2], T. Jensen[28], E. Joffrin[12], A. Kallenbach[2], J. Kalis[2], A. Kappatou[2], J. Karhunen[7], C.-P. Käsemann[2], S. Kasilov[56,57], Y. Kazakov[31], A. Kendl[17], W. Kernbichler[32], E. Khilkevitch[43], M. Kircher[2], A. Kirk[9], S. Kjer Hansen[44], V. Klevarova[30], F. Klossek[2], G. Kocsis[18], M. Koleva[2], M. Komm[48], M. Kong[16], A. Krämer-Flecken[13], M. Krause[2], I. Krebs[8], A. Kreuzeder[2], K. Krieger[2], O. Kudlacek[2], D. Kulla[5], T. Kurki-Suonio[7], B. Kurzan[2], B. Labit[16], K. Lackner[2], F. Laggner[35], A. Lahtinen[7], P. Lainer[32], P. T. Lang[2], P. Lauber[2], M. Lehnen[46], L. Leppin[2], E. Lerche[2], N. Leuthold[22], L. Li[13], J. Likonen[24], O. Linder[2], H. Lindl[2], B. Lipschultz[33], Y. Liu[22], Z. Lu[2], T. Luda Di Cortemiglia[2], N. C. Luhmann[34], T. Lunt[2], A. Lyssoivan[31], T. Maceina[2], J. Madsen[28], A. Magnanimo[2], H. Maier[2], J. Mailloux[9], R. Maingi[35], O. Maj[2], E. Maljaars[8], V. Maquet[31], A. Mancini[15], A. Manhard[2], P. Mantica[15], M. Mantsinen[36,59], P. Manz[58], M. Maraschek[2], C. Marchetto[40], M. Markl[32], L. Marrelli[11], P. Martin[11], F. Matos[2], M. Mayer[2], P. J. McCarthy[38], R. McDermott[2], G. Meng[2], R. Merkel[2], A. Merle[16], H. Meyer[9], M. Michelini[2], D. Milanesio[40], V. Mitterauer[2], P. Molina Cabrera[2], M. Muraca[2], F. Nabais[6], V. Naulin[28], R. Nazikian[35], R. D. Nem[28], R. Neu[2,39], A. H. Nielsen[28], S. K. Nielsen[28], T. Nishizawa[2], M. Nocente[47], I. Novikau[2], S. Nowak[15], R. Ochoukov[2], J. Olsen[28], P. Oyola[23], O. Pan[2], G. Papp[2], A. Pau[16], G. Pautasso[2], C. Paz-Soldan[22], M. Peglau[2], E. Peluso[29], P. Petersson[21], C. Piron[11], U. Plank[2], B. Plaum[27], B. Plöckl[2], V. Plyusnin[6], G. Pokol[18,25], E. Poli[2], A. Popa[2], L. Porte[16], J. Puchmayr[2], T. Pütterich[2], L. Radovanovic[32], M. Ramisch[27], J. Rasmussen[28], G. Ratta[51], S. Ratynskaia[21], G. Raupp[2], A. Redl[57], D. Réfy[18], M. Reich[2], F. Reimold[5], D. Reiser[13], M. Reisner[2], D. Reiter[13], B. Rettino[2], T. Ribeiro[2], D. Ricci[15], R. Riedl[2], J. Riesch[2], J. F. Rivero Rodriguez[23], G. Rocchi[53], P. Rodriguez-Fernandez[44], V. Rohde[2], G. Ronchi[8], M. Rott[2], M. Rubel[21], D. A. Ryan[9], F. Ryter[2], S. Saarelma[9], M. Salewski[28], A. Salmi[7], O. Samoylov[2], L. Sanchis Sanchez[23], J. Santos[6], O. Sauter[16], G. Schall[2], A. Schlüter[2], J. Scholte[8], K. Schmid[2], O. Schmitz[49], P. A. Schneider[2], R. Schrittwieser[17], M. Schubert[2], C. Schuster[2], N. Schwarz[2], T. Schwarz-Selinger[2], J. Schweinzer[2], F. Sciortino[2], O. Seibold-Benjak[2], A. Shabbir[30], A. Shalpegin[16], S. Sharapov[9], U. Sheikh[16], A. Shevelev[43], G. Sias[41], M. Siccinio[2], B. Sieglin[2], A. Sigalov[2], A. Silva[6], C. Silva[6], D. Silvagni[2], J. Simpson[9], S. Sipilä[7], A. Snicker[7], E. Solano[51], C. Sommariva[16], C. Sozzi[15], M. Spacek[2], G. Spizzo[11], M. Spolaore[11], A. Stegmeir[2], M. Stejner[28], D. Stieglitz[2], J. Stober[2], U. Stroth[2,10], E. Strumberger[2], G. Suarez Lopez[2], W. Suttrop[2], T. Szepesi[18], B. Tál[2], T. Tala[24], W. Tang[2], G. Tardini[2], M. Tardocchi[15], D. Terranova[11], M. Teschke[2], E. Thorén[21], W. Tierens[2], D. Told[2], W. Treutterer[2], G. Trevisan[11], M. Tripský[31], P. Ulbl[2], G. Urbanczyk[2], M. Usoltseva[2], M. Valisa[11], M. Valovic[9], S. van Mulders[16,46], M. van Zeeland[22], F. Vannini[2], B. Vanovac[44], P. Varela[6], S. Varoutis[20], T. Verdier[28], G. Verdoolaege[30,31], N. Vianello[11], J. Vicente[6], T. Vierle[2], E. Viezzer[23], I. Voitsekhovitch[9], U. von Toussaint[2], D. Wagner[2], X. Wang[2], M. Weiland[2], D. Wendler[2,10], A. E. White[44], M. Willensdorfer[2], B. Wiringer[2], M. Wischmeier[2], R. Wolf[5], E. Wolfrum[2], Q. Yang[42], C. Yoo[44], Q. Yu[2], R. Zagórski[19], I. Zammuto[2], T. Zehetbauer[2], W. Zhang[42], W. Zholobenko[2], A. Zibrov[2], M. Zilker[2], C. F. B. Zimmermann[2,10], A. Zito[2], H. Zohm[2] & S. Zoletnik[18]

[5]Max-Planck-Institut für Plasmaphysik, Greifswald, Germany. [6]Instituto de Plasmas e Fusão Nuclear, Instituto Superior Técnico, Universidade de Lisboa, Lisbon, Portugal. [7]Department of Applied Physics, Aalto University, Helsinki, Finland. [8]Eindhoven, University of Technology, Eindhoven, The Netherlands. [9]CCFE, Culham Science Centre, Abingdon, UK. [10]Physik-Department E28, Technische Universität München, Garching, Germany. [11]Consorzio RFX, Padova, Italy. [12]CEA/IRFM, Saint Paul Lez Durance, France. [13]Forschungszentrum, Jülich, Germany. [14]Institut Jean Lamour, Université de Lorraine, Nancy, France. [15]ENEA, IFP-CNR, Milan, Italy. [16]Ecole Polytechnique Fédérale

de Lausanne (EPFL), Swiss Plasma Center (SPC), Lausanne, Switzerland. [17]ÖAW, IAP, University of Innsbruck, Innsbruck, Austria. [18]Centre for Energy Research, Budapest, Hungary. [19]Institute of Plasma Physics and Laser Microfusion, Warsaw, Poland. [20]Karlsruhe Institut für Technologie, Karlsruhe, Germany. [21]KTH Royal Institute of Technology, Stockholm, Sweden. [22]General Atomics, San Diego, CA, USA. [23]Universidad de Sevilla, Sevilla, Spain. [24]VTT Technical Research Centre of Finland, Helsinki, Finland. [25]Budapest University of Technology and Economics, Budapest, Hungary. [26]Laboratoire de Physique Des Plasmas, Ecole Polytechnique, Palaiseau, France. [27]IGVP Universität Stuttgart, Stuttgart, Germany. [28]Department of Physics, Technical University of Denmark, Kgs. Lyngby, Denmark. [29]Department of Industrial Engineering, University of Rome, Rome, Italy. [30]Ghent University, Ghent, Belgium. [31]ERM/KMS, Brussels, Belgium. [32]ÖAW, IAP, Vienna University of Technology, Vienna, Austria. [33]York Plasma Institute, University of York, York, UK. [34]Electrical and Computer Engineering, University of California, Davis, CA, USA. [35]Princeton Plasma Physics Laboratory, Princeton, NJ, USA. [36]Barcelona Supercomputing Center, Barcelona, Spain. [37]ENEA Consorzio CREATE, Naples, Italy. [38]School of Physics, University College Cork, Cork, Ireland. [39]Technische Universität München, Garching, Germany. [40]ISC-CNR and Politecnico di Torino, Torino, Italy. [41]Department of Electrical and Electronic Engineering, University of Cagliari, Cagliari, Italy. [42]Chinese Academy of Sciences, Hefei, China. [43]Ioffe Institute, St. Petersburg, Russian Federation. [44]MIT Plasma Science and Fusion Center, Cambridge, MA, USA. [45]Modeling Group, École Supérieuré d'ingénieurs Léonard-de-Vinci, Courbevoie, France. [46]ITER Organization, Saint-Paullez-Durance, France. [47]ENEA, University of Milano-Bicocca, Milano, Italy. [48]Institute of Plasma Physics of the CAS, Praha, Czech Republic. [49]University of Wisconsin, Madison, WI, USA. [50]Department of Physics, Chalmers University of Technology, Gothenburg, Sweden. [51]Laboratorio Nacional de Fusión, CIEMAT, Madrid, Spain. [52]Department of Physics, Durham University, Durham, UK. [53]ENEA, Centro Ricerche Frascati, Frascati, Italy. [54]Aix-Marseille University, CNRS, Marseille, France. [55]Institute of Plasma Physics, National Science Center Kharkov Institute of Physics and Technology, Krakov, Ukraine. [56]ÖAW, Graz University of Technology, Graz, Austria. [57]DEIM Department, Università degli Studi della Tuscia, Viterbo, Italy. [58]Universität Greifswald, Greifswald, Germany. [59]ICREA, Barcelona, Spain.